FEBS Open Bio 4 (2014) 496–509

FEBS openbio

journal homepage: www.elsevier.com/locate/febsopenbio

Molecular mechanisms in the selective basal activation of pyrabactin receptor 1: Comparative analysis of mutants

Lyudmyla Dorosh [a,c], Nandhakishore Rajagopalan [b], Michele C. Loewen [b,d], Maria Stepanova [a,c,*]

[a] National Research Council of Canada, Edmonton, Alberta, Canada
[b] National Research Council of Canada, Saskatoon, Saskatchewan, Canada
[c] Department of Electrical and Computer Engineering, University of Alberta, Edmonton, Alberta, Canada
[d] Department of Biochemistry, University of Saskatchewan, Saskatoon, Saskatchewan, Canada

ARTICLE INFO

Article history:
Received 21 March 2014
Revised 10 May 2014
Accepted 13 May 2014

Keywords:
Pyrabactin resistance
Abscisic acid signaling
Constitutively active mutations
Molecular dynamics simulations
Essential collective dynamics analysis

ABSTRACT

Pyrabactin receptors (PYR) play a central role in abscisic acid (ABA) signal transduction; they are ABA receptors that inhibit type 2C protein phosphatases (PP2C). Molecular aspects contributing to increased basal activity of PYR against PP2C are studied by molecular dynamics (MD) simulations. An extensive series of MD simulations of the apo-form of mutagenized PYR1 as a homodimer and in complex with homology to ABA-insensitive 1 (HAB1) phosphatase are reported. In order to investigate the detailed molecular mechanisms mediating PYR1 activity, the MD data was analyzed by essential collective dynamics (ECD), a novel approach that allows the identification, with atomic resolution, of persistent dynamic correlations based on relatively short MD trajectories. Employing the ECD method, the effects of select mutations on the structure and dynamics of the PYR1 complexes were investigated and considered in the context of experimentally determined constitutive activities against HAB1. Approaches to rationally design constitutively active PYR1 constructs to increase PP2C inhibition are discussed.

1. Introduction

In 2009, two research groups independently reported the discovery of a family of abscisic acid (ABA) -binding proteins in *Arabidopsis thaliana*, containing as many as 14 members known as PYR1 (pyrabactin resistance 1) and PYL (PYR1-like) [1] or RCAR (regulatory component of ABA response) receptors [2]. In one instance this was enabled by the identification of pyrabactin as an inhibitor of ABA-mediated developmental and stress response effects in phenotypic screens [1]. Pyrabactin was shown to mediate its inhibition through the pyrabactin receptor 1 protein (PYR1). Further analyses showed that PYR1 and its associated homologs play a central role in ABA signal transduction, as the ABA receptors, acting via inhibition of protein phosphatases of the type 2C (PP2C) variety [1–3].

Structural studies have demonstrated that when ABA binds to the receptor, interactions between the agonist and two flexible loops (Lβ3β4 and Lβ5β6 named gate and latch, respectively) form a unique receptor surface (Fig. 1A) that can interact with the phosphatases [4,5]. Three independent studies also demonstrated that a subset of the ABA receptors exhibit constitutive activity against PP2Cs *in vitro* [1,6,7]. Although PYR1 and PYLs 1–3 show very weak basal activity, PYL4 was found to be active against HAB1 [7], whereas other family members such as PYLs 5–6 and 8–10 are constitutively active. Based on analogy to the PYL10's gate sequence, recent work demonstrated that replacing residue V87 in PYL2's gate-latch region by the bulkier L87 equivalent from PYL10 partially increased PYL2's constitutive inhibition of PP2C [7]. Further in this vein, a less rational but more successfully applied broad based mutagenic screening approach to the development of constitutive active ABA receptors was recently reported [8]. In this instance probing of 39 residues around ligand pocket in the ABA receptor led to the identification of 10 sites in the gate-latch and C-terminal helix regions involved in mediating basal receptor activity. Interestingly, although single-site mutations were sufficient to

Abbreviations: MD, molecular dynamics; ECD, essential collective dynamics; PCA, principal component analysis; WT, wild type; ABA, A8S abscisic acid; PDB, Protein Data Bank; PP2C, phosphatase type 2C; PYR1, pyrabactin resistance 1; PYL, PYR1-like; RCAR, regulatory component of ABA response; CA, constitutively active; HAB1, homology to ABA insensitive 1; PYV, pyrabactin or $C_{16}H_{13}BrN_2O_2S$; P2M, *N*-(pyridin-2-ylmethyl) naphthalene-1-sulfonamide or $C_{16}H_{14}N_2O_2S$

* Corresponding author at: Department of Electrical and Computer Engineering, University of Alberta, 9107-116 Street, Edmonton, Alberta, Canada.
E-mail address: ms1@ualberta.ca (M. Stepanova).

http://dx.doi.org/10.1016/j.fob.2014.05.001
2211-5463/

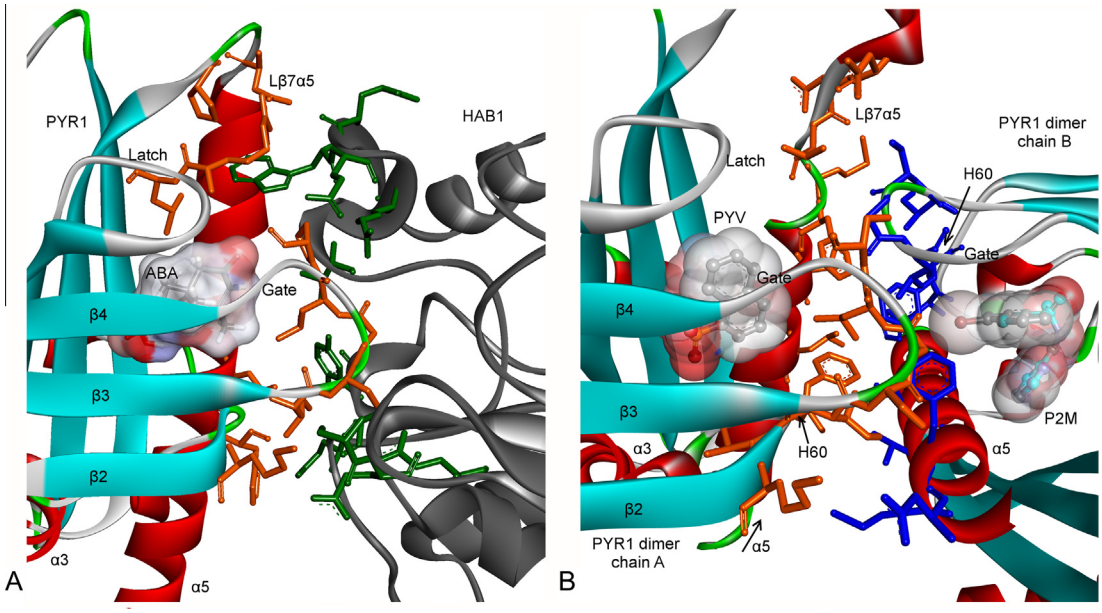

Fig. 1. PYR1 residues comprising the binding interfaces [10]: (A) – in PYR1–ABA–HAB1 complex, PDB ID 3QN1, with orange sticks showing PYR1 residues and green sticks showing HAB1 residues; and (B) – in PYV/P2M-bound PYR1 dimer, PDB ID 3NJO, with orange and blue sticks showing the residues of chain A and B, respectively. The ligands are depicted by translucent surfaces, colored according to the charge of ligand's atoms: red – positive charge, blue – negative charge, white – no charge. (For interpretation of the references to color in this figure legend, the reader is referred to the web version of this article.)

stabilize receptor-PP2C interactions (as detected by yeast-2-hybrid analysis), stacking of 3 and even 4 mutations was necessary to elicit basal receptor activation at a level comparable to ABA-stimulated receptor activity *in vitro*.

Recently it was demonstrated that ABA-receptors can adopt a homodimeric form in solution (in the absence of ABA, see Fig. 1B) and that this dimerization correlates with inhibition of basal receptor activity. In particular, ABA-free PYR1, PYL1 and PYL2 were found to be homodimeric, whereas PYLs 5–6 and 8–10 adopt a preferentially monomeric form [9,7]. It has also been shown [7] that mutation I88K in PYL2 both prevents homodimer formation in solution and increases its constitutive activity. Residue 60 in PYR1 has also been found to play a key role in determining the ABA-bound receptors' oligomeric state [9].

Molecular dynamics (MD) simulations and associated essential collective dynamics (ECD) analyses of wild type (WT) PYR1 in homodimeric and PP2C complexes reported in our earlier study [10], further support a 'competing complexes' model in which PYR1–PYR1 dimerization might be in competition with formation of PYR1–HAB1 complexes, in particular in the absence of ABA. Addition of ABA yielded an opposite effect on the dynamics of PYR1–HAB1 and PYR1–PYR1 complexes, constraining inter-molecular interactions in the former and destabilizing the latter. An in depth description of the ECD framework is available elsewhere [10–14].

Now, MD simulations and associated ECD analyses of mutations demonstrated, or predicted, to promote dissociation of the PYR1–PYR1 dimer or promote the constitutively active association of PYR1 with HAB1 are reported. Extensive MD simulations and experiments for multiple mutants of PYR1 considered in the context of complex formation with HAB1 versus homodimer were undertaken. Employing the ECD framework we investigate the effects of the mutations on structure and dynamics of the PYR1 complexes. We discuss promising PYR1 mutations and approaches to design constitutively active PYR1 constructs.

2. Results and discussion

2.1. Analysis of constitutively active PYR1 mutant constructs

A comparison of the interacting surfaces for PYR1 dimers versus the PYR1–ABA–HAB1 complex [3,15,16], based on our MD simulations analyses discussed elsewhere [10], shows that the interfaces are largely the same in these two complexes. Examples of PYR1 binding areas in crystallographic structure of in ABA-bound complex with HAB1 (PDB ID 3QN1) and PYV/P2M-bound dimer (PDB ID 3NJO) shown in Fig. 1A and B, respectively, indicate that the binding areas overlap significantly. PYR1 residues involved in these interactions, as identified by Accelrys VS, are listed in Table 1. The table also presents the inter-molecular interaction data for apo-PYR1 dimer for original X-ray crystallographic structure PDB ID 3K3K, as well as PYR1 residues contacting ABA for structure PDB ID 3K3K. It can be seen that similar interactions are found in loops Lα3β2, Lβ3β4, the gate, and helix α5 in PYR1–ABA–HAB1 complex and in both dimers. In apo-dimer, also the latch and the area of helix Lβ7α5 are involved in the interactions, similarly to the PYR1–ABA–HAB1 complex. A detailed comparative analysis of these interactions is presented elsewhere [10].

The overlap of the binding areas in PYR1 complexes with HAB1 and in the dimers complicates the task of identifying CA mutations of PYR1 that might drive it to preferentially bind to PP2Cs over forming homodimers in the absence of ABA. Thus activity and structural information from published reports [8,18], as well as available crystallographic structural data about ligand binding sites in PYL10 [7], residues involved in intermolecular interactions of PYL2 dimers [18] and interactions with phosphatase [18] were also considered. Fig. S1 (Suppl. Mat.) presents a sequence alignment for selected relevant PYR/PYL constructs, highlighting 42 identified sites involved in ligand (L), HAB1 phosphatase (P), or intermolecular dimer (D) PYR1 contacts. A detailed discussion of the considerations of these sites leading to the

Table 1
PYR1 residues involved in strong interactions in binding areas of PYR1–PYR1 and PYR1–ABA–HAB1 complexes, and residues interacting with ABA in PYR–ABA complex. The donors or acceptors in hydrogen bonds have been identified within a 3.5 Å cutoff in ligand pocket. Other close neighbors of ABA have been identified within a 4 Å cutoff. The activation mutations are from [6–9,18,15,16]. Round brackets indicate similar mutation sites for PYL2/PYL1.

PYR1 structure element	Interactions PYR1/PYR1 dimer & PYV	Interactions PYR1/PYR1 dimer apo	Interactions PYR1/HAB1 ABA bound	PYR1 neighbors of ABA	Constitutively active (CA) mutations	Activation mutations & ABA/PYV
Reference structure	3NJO.pdb [16]	K3K.pdb [17]	3QN1.pdb [15]	3K3K.pdb [17]	[8]	[6–9,18,15,16]
Lα3β2	K63	H60, F61, K63	H60, F61, K63	K59, F61	H60, (F61)	F61, (I62)
Lβ3β4	I84	I84	I84	V83	V83, I84	
Gate	S85, L87	G86, P88	S85, G86, L87, P88	L87, P88, A89	L87, A89	S85, L87, P88, (A89)
β4, β5				S92, E94, F108, I110		E94, (I110)
Latch		R116	R116, L117	H115, R116, F117,		R116
β6, β7				Y120, S122, E141		Y120, E141
Lβ7α5		N151	P148, N151		(N151)	S152
α5	D155, M158	D155, M158, F159	D155, M158, F159	F159	M158, F159	R157H, (A160)
α5	L166	V163, L166	T162, L166	V163	T162, L166	(V163)
α5	Q169	Q169		N167, Q169	K170	

exclusion of 23 of them from further testing is included in the caption of Fig. S1.

Two types of CA inducing mutations can be envisioned based on the 'competing complexes' model, including PYR1 dimer destabilizing mutations versus mutations which enhance basal PYR1 interactions with PP2C. The first type would require mainly non-conservative mutations to drastically change the position of side chains of neighboring residues at the core of the dimerization interface [19]. To date, two types of dimer destabilizing mutations have been characterized; both involving residues from the remaining 19 potential CA mutation sites. These include mutation H60P in the Lα3β2 region [9] and mutations in the C-terminal helix, such as K170W, L166F, T162F, or M158I, and also F159V [8]. The M158I and F159V pair is included in all CA mutant sets tested by Mosquna et al. [8]. Structural considerations suggest these mutations potentially lead to residue 158 being uniquely exposed at the binding interface and residue 159 being buried behind neighboring residue A160 in the ligand pocket, yielding a surface that could inhibit dimer formation. Additional insight into potential dimer-dissociating mutations was gained upon consideration of the sequences of other PYL receptors, such as PYL6 and PYL10, which show substantially higher basal activity in comparison to PYR1 [7]. Sequential sequence differences suggest that mutation K170W (polymorphism K170S) as well as D155E and D154E are likely primary factors defining monomericity of PYR/PYL receptors when histidine is retained at position 60, as in PYL6. The second type of mutations, to enhance the PYR1–PP2C interaction, could be envisioned in two distinct regions including, the gate-latch and the N-terminal part of helix α5. For example gate-mutations such as V83F, L87F, or A89W replace hydrophobic, non-polar residues with bigger and even more hydrophobic side chains which tend to be involved in stabilizing stacking interactions. Interestingly, it has been shown that it is more efficient to make only one or two mutations per element of secondary structure of interest, potentially because excessive additional volume cannot be accommodated [8]. Finally, as an alternative, exploiting non-conservative substitutions in regions distal from ligand or protein interaction surfaces, by analogy with strongly CA PYL6 and PYL10, was also investigated. Toward this, the set of potential activation sites was extended to include those with minor allele frequencies including R50, D53, T93, and V138 (Suppl. Mat. Fig. S2).

All together, ten conservative and non-conservative amino acid substitutions, R50S, D53E, H60P, V83I, V83F, L87I, T93L, V138R, F158I, and V159V, were constructed by *in silico* mutagenesis which may be expected to favor the closed lid conformation in ABA-free PYR1, or imitate strong inter- and intra-protein correlations observed in the PYR1–ABA–HAB1 complex, or else destabilize the ABA-free dimer. Four mutation sets were analyzed numerically in this paper. In particular, Models 1 and 2 represent previously reported mutated PYR1 constructs H60P [9] and H60P V83F M158I F159V [8], respectively. Models 3 and 4 comprise sets of mutations R50S D53E T93L V138R and D53E H60P V83I L87I F159V, which have not been explored before. Furthermore, Models 2, 3, and 4 were also assessed experimentally. Below we report results of these experiments as well as a comparative MD simulation ECD analysis of these sets of mutations.

2.2. Constitutive activity of PYR1 mutants

The constitutive activity of PYR1 and its mutants were analyzed using the phosphatase activity assay. 1:2.5 and 1:25 M ratios of phosphatase: receptors were tested in these assays. CA receptors are expected to show a reduction of phosphatase activity even in the absence of (+) ABA. PYR1 showed no constitutive activity at both ratios, while Model 2 showed high constitutive activity even at the lower molar ratio and inhibited phosphatase activity to the same level as ABA (Fig. 2). Model 3 did not show any constitutive activity at both the molar ratios tested. Finally Model 4 was not active at the lower molar ratio of 1:2.5, however, at higher molar ratio of 1:25, it showed nearly 60% inhibition of phosphatase activity (Fig. 2). All four proteins showed similar responses to ABA showing that they were all functionally active as ABA receptors. Overall this set of mutant PYR1 models present an array of CA activities for comparative investigation by MD simulations and ECD analyses.

2.3. Comparative ECD analysis of mutant and wild type PYR1 complexes

For each of the four mutated models, ECD analysis of 100 segments of the corresponding MD trajectories was performed and results averaged as described in Section 3. Comparisons of the ECD descriptors for the mutants in the form of ABA-free PYR1 dimers and PYR1–HAB1-complexes with respect to WT PYR1 equivalents from [10] were made to interpret the experimental observations as well as further clarify the mechanisms associated with mutations that would mimic the dynamics of the PYR1–ABA–HAB1 complex in the absence of ABA while destabilizing the ABA-free dimer construct as much as possible.

2.3.1. Model 1

Model 1 contains a single dimer destabilizing mutation H60P, which has been characterized previously *in vitro* and is expected to weaken affinity in the dimer [9]. Thus the numerical analysis

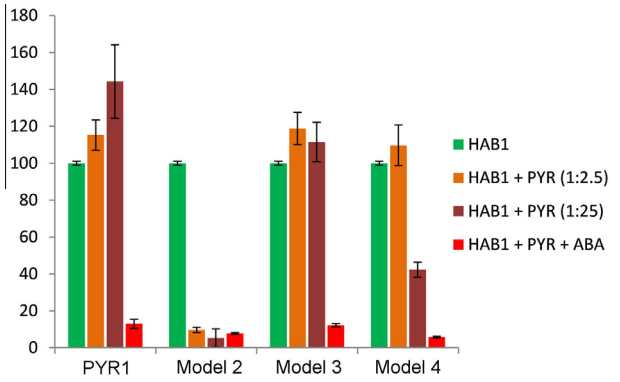

Fig. 2. *In vitro* phosphatase assay of HAB1 alone (green bars), HAB1 + PYR (1:2.5 ratio) (orange), HAB1 + PYR (1:25 ratio) (brown) and HAB1 + PYR (1:2.5 ratio) + 1 μM (+) ABA (red bars). The fluorescence of HAB1 alone was set as 100%. Each bar shows the average % activity of three replicates and ±standard deviation. (For interpretation of the references to color in this figure legend, the reader is referred to the web version of this article.)

of its dynamics presents an important benchmark example for the following discussion of other mutated constructs. The PYR1 ABA-free dimer and PYR1–HAB1 binding interfaces for Model 1 are shown in Fig. 3, panels (A) and (B), respectively. In PYR1 dimer, mutation H60P affects the orientation of neighboring residue F61, preventing binding to Lβ3β4 and the N-terminus of helix α5 (P88(B)–M158(A)) asymmetrically. However, a close contact persists at the interface of mutant dimer (Fig. 3A). As concerns the PYR1–HAB1 binding interface, mutation H60P prevents F61 from binding to residues E323 and Y404 of the phosphatase (Fig. 3B).

Fig. 4 compares the ECD main chain flexibilities profiles for a WT PYR1 dimer containing two ABA molecules, denoted here as 2ABA-bound PYR1 dimer, with WT ABA-free apo dimer and ABA-free Model 1 mutant dimer. In the flexibility profiles, peaks of the descriptor $F_i^{C_\alpha}$ are usually observed in the areas of flexible loops of the protein, whereas minima or low-leveled plateaus, as a rule, correspond to more rigid β-sheets or α-helices. As it can be seen from Fig. 4, loops Lα1β1, Lβ2β3 and Lβ6β7, as well as C-terminus of helix α5 exhibit a high flexibility for all three PYR1 systems in Fig. 4; the latch is pronouncedly flexible in 2-ABA bound dimer, but to a lesser extent in the apo-dimers; whereas the flexibility maximum in the area of loop Lβ7α5 is somewhat shifted toward the N-terminus, particularly in the case of two WT systems. Fig. 4 also shows that the main chain flexibility of ABA-free H60P mutant dimer (Model 1) is very close to that of 2ABA-bound and ABA-free WT dimers, except for regions near the gate and the latch, Lβ7α5, C-terminal part of α-helix α5, and residues 20–35. Interestingly, the flexibilities of chains A in both mutated Model 1 and WT ABA-free dimers exhibit a pronounced plateau in the regions of the latch and C-terminus of helix α5. In WT 2ABA-bound dimer, high flexibility in the latch region is related to the interaction of P88 with ABA, resulting in a decoupling of loop Lβ5α4 and helix α4 (the latch) from the rest of PYR1. Since mutation H60P results in a similar flexibility profile, the mutation evidently affects not only the neighboring F61, but also influences relatively distant residue P88. The flexibility of chain A Model 1 mutant dimer is higher in the region of residues 148–151, which is attributable to disruption of bonds at residues N151 and P148. All profiles in Fig. 4 show a low flexibility of critical regions around residue 60 and N-terminus of helix α5, while in the area of the gate the flexibility of Model 1 dimer is slightly lower than that of both WT dimers. In the area of the latch, flexibility of chain A in Model 1 dimer is slightly lower than that in WT apo-dimer and pronouncedly lower than in 2ABA-bound dimer. The main chain flexibilities of chains B in the three dimer systems are shown on Fig. S3 (Suppl. Mat.). From comparison of the plots in Fig. 4 and Fig. S3 it is evident that the presence of the ligand or mutation affects dynamics of the chains asymmetrically. In distinction to chain A, the flexibility profiles of chain B in all three dimer systems are almost identical, with an exception of slightly higher flexibility of loop Lβ7α5 in 2ABA-bound WT dimer and slightly higher flexibility of loop Lβ6β7 in Model 1 mutant.

Complementary to the ECD flexibility profiles, we have also analyzed C_α atoms correlation maps (see Section 3 for technical details).

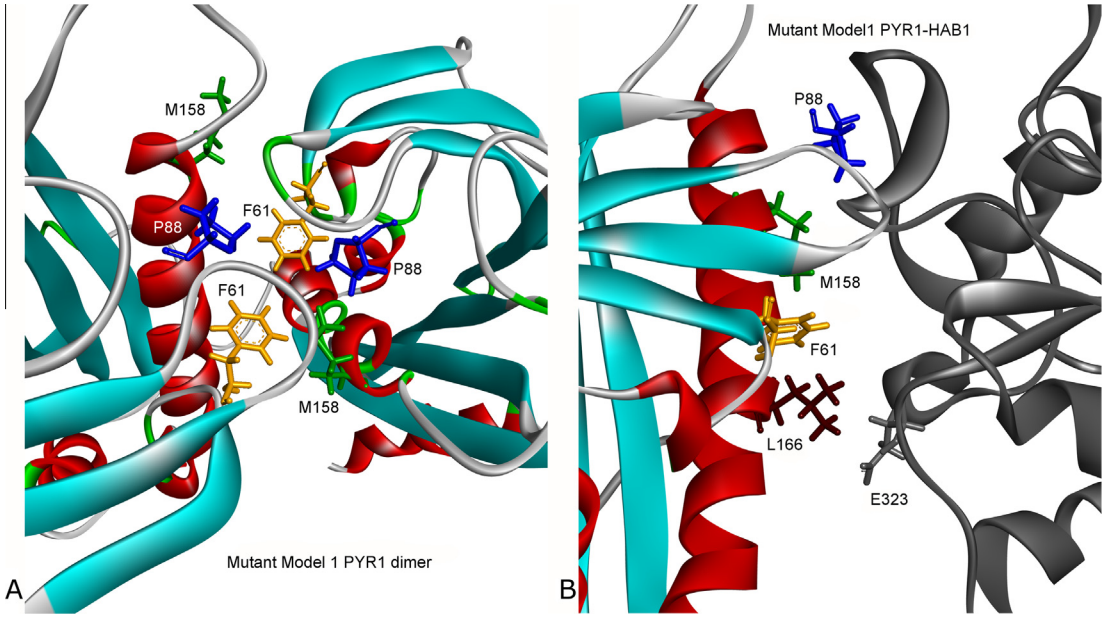

Fig. 3. Close up of the binding area for ABA-free dimer (A) and ABA-free PYR1–HAB1 complex (B) from MD simulations using Accelrys VS for Model 1. The important residues on binding surfaces are indicated according to [8]. The PYR1's F61 are depicted with yellow sticks, P88 with blue sticks and the residues M158 are depicted with green sticks. In (A), the mutation H60P in dimer affects the orientation of the main chain A around residue F61, which repels chain B residue F61. The same mutation in the PYR1–HAB1 complex in (B) can also prevent bonds formation between residues F61, L166 (not shown), and Y404 (not shown), E323 (depicted with gray sticks). (For interpretation of the references to color in this figure legend, the reader is referred to the web version of this article.)

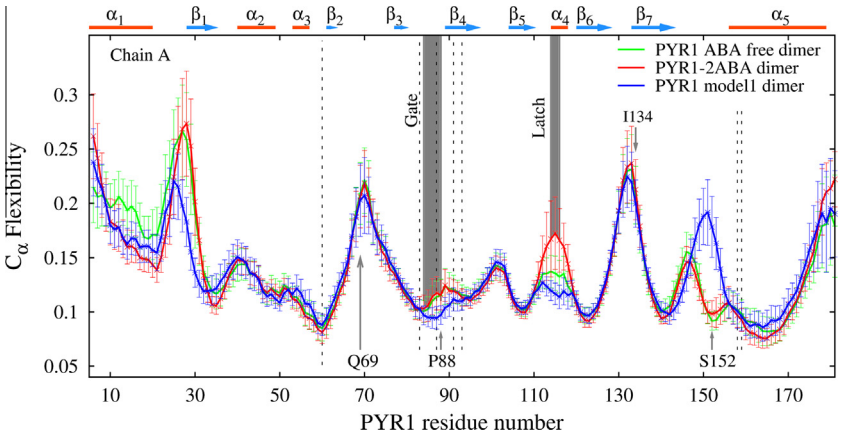

Fig. 4. PYR1 main chain flexibility profiles for chain A of dimer constructs: WT ABA-free (green line), WT 2ABA-bound (red line), and ABA-free H60P mutant (denoted as Model 1, blue line). Vertical dashed lines indicate the potential mutation sites and regions of phosphatase binding. (For interpretation of the references to color in this figure legend, the reader is referred to the web version of this article.)

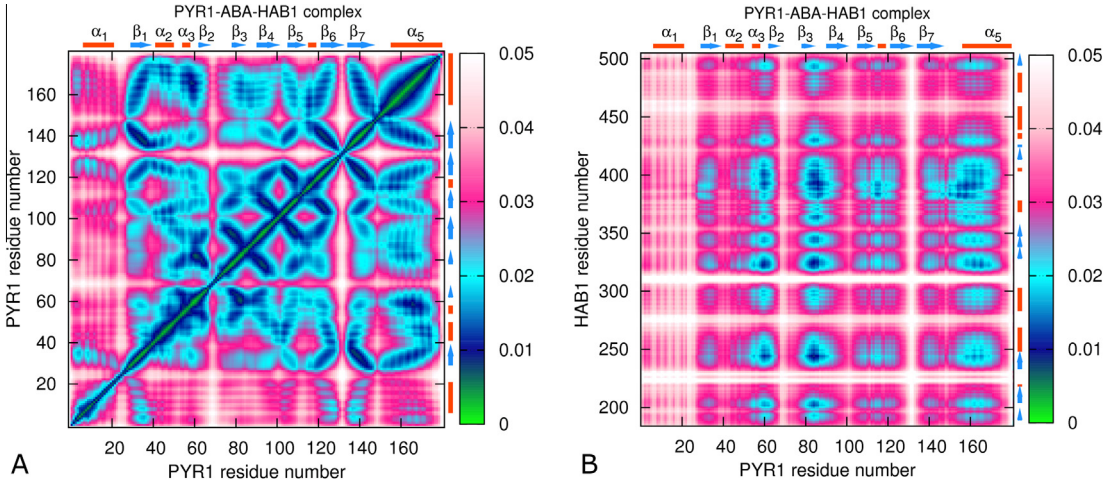

Fig. 5. C_α atoms correlation maps for intra-receptor (A) and inter-molecular (B) correlations in WT PYR1–ABA–HAB1 complex. Strong correlations are shown in green and dark blue colors (low levels of the correlation descriptor), while weaker correlations are shown with white and light magenta colors (high levels of the descriptor, see also Section 3). (For interpretation of the references to color in this figure legend, the reader is referred to the web version of this article.)

Examples of intra-molecular and inter-molecular correlation maps for the PYR1–ABA–HAB1 complex are shown in Fig. 5A and B, respectively. The maps represent correlations between main chain carbon atoms, including direct contacts, steric constraints and water- or ions-mediated secondary interactions. One can see strong intra-molecular correlations for all structural elements of PYR1 in region of residues 26–180, whereas the areas of loops Lα3β2, β3β4, the latch, sheet β7, and helix α5 show strong inter-molecular correlations with HAB1 residues. In order to facilitate the comparative analysis of PYR1 mutants dynamics, difference correlation maps were also analyzed for the various complexes relative to a control construct, as described in Section 3. Fig. 6A–D present examples of difference correlation maps for intra-molecular correlations (A,C) and inter-molecular correlations (B,D) in WT PYR1 dimer (A,B) and PYR1–HAB1 complex (C,D) (for dimers ABA-free (apo) WT PYR1–PYR1 constructs were used as a control, whereas for PYR1–HAB1 complexes ABA-bound WT PYR1–ABA–HAB1 constructs were used as a control). In the dimer system, according to Fig. 6A, binding of two ABA molecules weakens intra-molecular correlations of the latch with the rest of receptor, but strengthens the correlations in the area of helix α1. The corresponding changes of inter-molecular correlations (Fig. 6B), in turn, are asymmetrical and show a partial loss of correlations at the latch in chain A and around the loops Lβ3β4 and Lβ7α5 as well as the latch in chain B. In PYR1–HAB1 complex, absence of ABA decreases PYR1 intra-molecular correlations in helix α5 and at the latch, but strengthens correlations of helix α1 with the rest of the molecule (Fig. 6C). Finally, inter-molecular correlations of PYR1 in ABA-free PYR1–HAB1 complex are weakened at various locations, in particular with HAB1's regions around 460, 310, 280 and 230. Interestingly, all these residues are located on loops distant from the binding surface. One can infer that absence of ABA indirectly affects the dynamics of distant regions of HAB1.

Fig. S4A and S4B present difference intra-molecular and inter-molecular correlation maps for the mutant Model 1 dimer against WT ABA-free dimer complex (control). It can be seen that Model 1 exhibits a partial loss of intra-receptor correlations in the regions of the loop Lβ7α5 and helix α5 of the dimer (red colored areas in Fig. S4A). This loss of correlation is consistent with the Lβ7α5 decoupling observed in the dimer flexibility profile for Model 1 (Fig. 4). At the same time, stronger inter-molecular correlation between N-terminal helix α1, loops Lα1β1 and Lβ3β4 and also the latch of chain A with β-sheets and helices α1 and α5 of chain B is observed in Model 1 in comparison with the WT apo-dimer (see green colored areas in Fig. S4B).

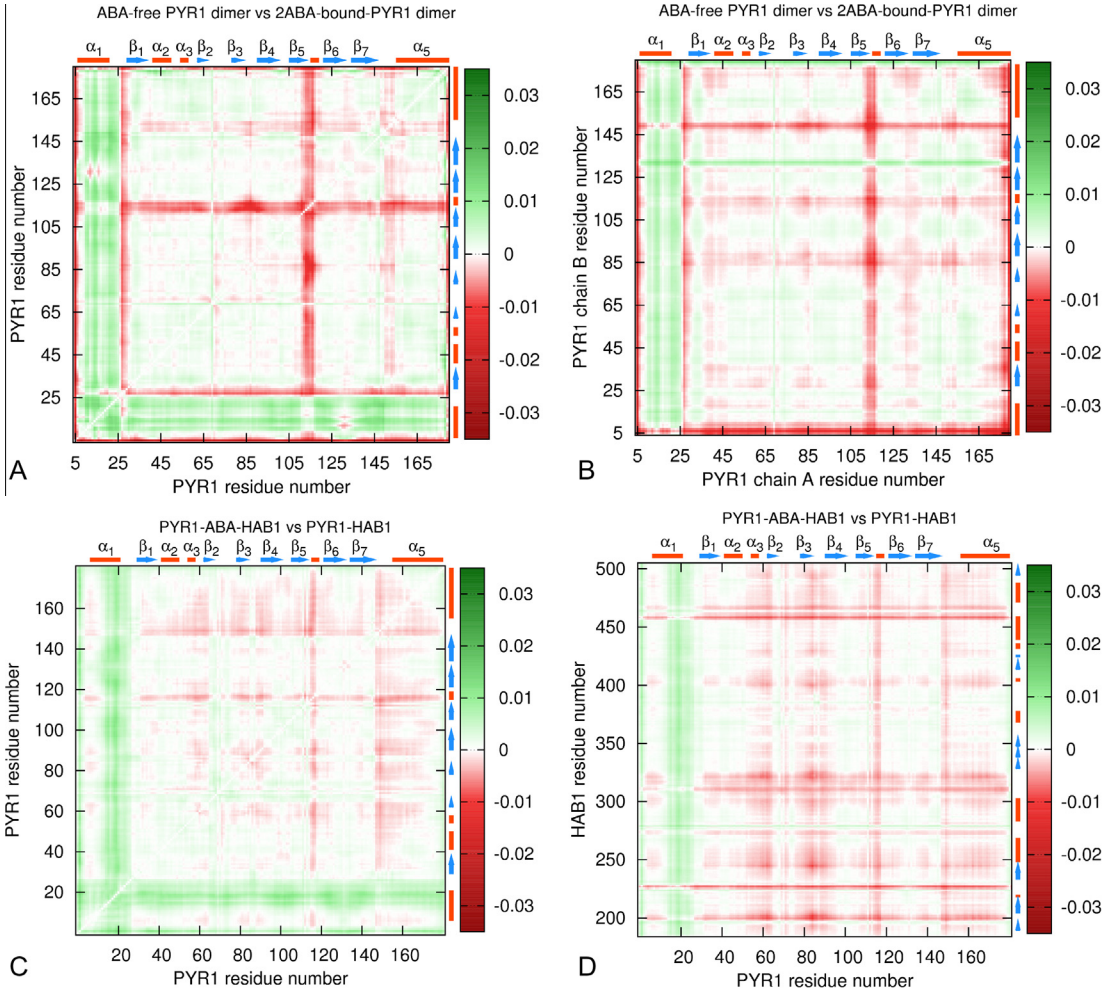

Fig. 6. Difference intra-molecular (A, C) and inter-molecular (B, D) C_α atoms correlation maps relative to control for 2ABA-bound PYR1 dimer (A, B) and ABA-free PYR1–HAB1 complex (C, D); intra-molecular correlation maps were built for chain A residues of dimer (A), while inter-molecular correlation maps present chain A residues on horizontal axis and chain B on vertical axis (B). For control, ABA-free PYR1 dimer was used in (A, B) and PYR1–ABA–HAB1 complex in (C, D). In the difference maps, green color indicates stronger correlation than in the control, and red color indicates less constrained and more flexible regions than in the control. White color indicates regions with the same level of correlations. (For interpretation of the references to color in this figure legend, the reader is referred to the web version of this article.)

Since potential CA mutations are expected to imitate the dynamics of the PYR1–ABA–HAB1 complex in the absence of ABA, we have also compared the flexibility profiles and correlation maps of ABA-free, Model 1 mutant PYR1–HAB1 construct with the WT ABA-bound construct. Fig. S5 compares the corresponding flexibility profiles for both PYR1 and HAB1 main chains; Fig. S6A presents the difference intra-molecular correlation map for PYR1 in PYR1–HAB1 complex; and Fig. S6B shows the difference inter-molecular correlation map for this complex. As one can see from Fig. S5, in ABA-free H60P mutant the main-chain flexibility of HAB1 is considerably increased around residues G226, N227, S228, and N458. The corresponding loops are situated at the opposite side from the binding area of the phosphatase with PYR1, indicating that even a single mutation in ABA-free receptor may affect the dynamics of very distant regions of the phosphatase. From Fig. S5 it is evident that mutant Model 1 PYR1 residues shows encouraging agreement with the flexibility profile of WT PYR1–ABA–HAB1 construct. However, the correlation maps in Fig. S6 (A, B) reveal differences. For example, mutant Model 1 shows slightly weaker intra-PYR1 correlations in the loops Lβ7α5 and Lβ6β7 than observed in WT ABA-bound complex (Fig. S6A). Stronger inter-molecular correlations is observed between PYR1's alpha-helix α1 and sheet β2 with most HAB1 residues, whereas correlation with HAB's residues G226 and N458 (situated distantly from the binding surface area) is weakened strongly for all residues of PYR1 (Fig. S6B). Mutation Model 1 reproduces reasonably well the coupling of the latch, sheet β7, and helix α5 with HAB1 residues 230–420 as found in PYR1–ABA–HAB1 complex, however it fails to reproduce some of the strong correlations for the loops Lα3β2, Lβ3β4 and Lβ6β7 with the phosphatase (Fig. S6B).

One can conclude that Model 1 weakens inter-molecular correlations around sheets β1, β5, and β7, and helices α3 and α5 in the dimer, however it tends to loosen PYR1 bonding with HAB's N-ter and C-ter residues in the mutant apo-PYR1–HAB1 complex in comparison to WT PYR1–ABA–HAB1 complex (see Fig. S4B and S6B). In dimer, mutation H60P has been shown to affect the orientation of residue F61 in chain A, which repels chain B's residue F61 [9], however our analysis indicates that this does not decrease significantly the inter- and intra-molecular correlations in the area of loop Lα3β2. In the PYR1–HAB1 complex, mutation H60P slightly weakens the correlation between PYR1 region around residue F61 (loop Lα3β2) and all HAB1 residues except N277 and H224.

2.3.2. Models 2 and 4

Out of all mutated constructs, the closest dynamical matches to the WT PYR1–ABA–HAB1 system was achieved with Model 2 (H60P, V83F, M158I, F159V) [8] and Model 4 (D53E, H60P, V83I, L87I, F159V). Fig. 7 (A, B) and (C, D) present PYR1–PYR1 and

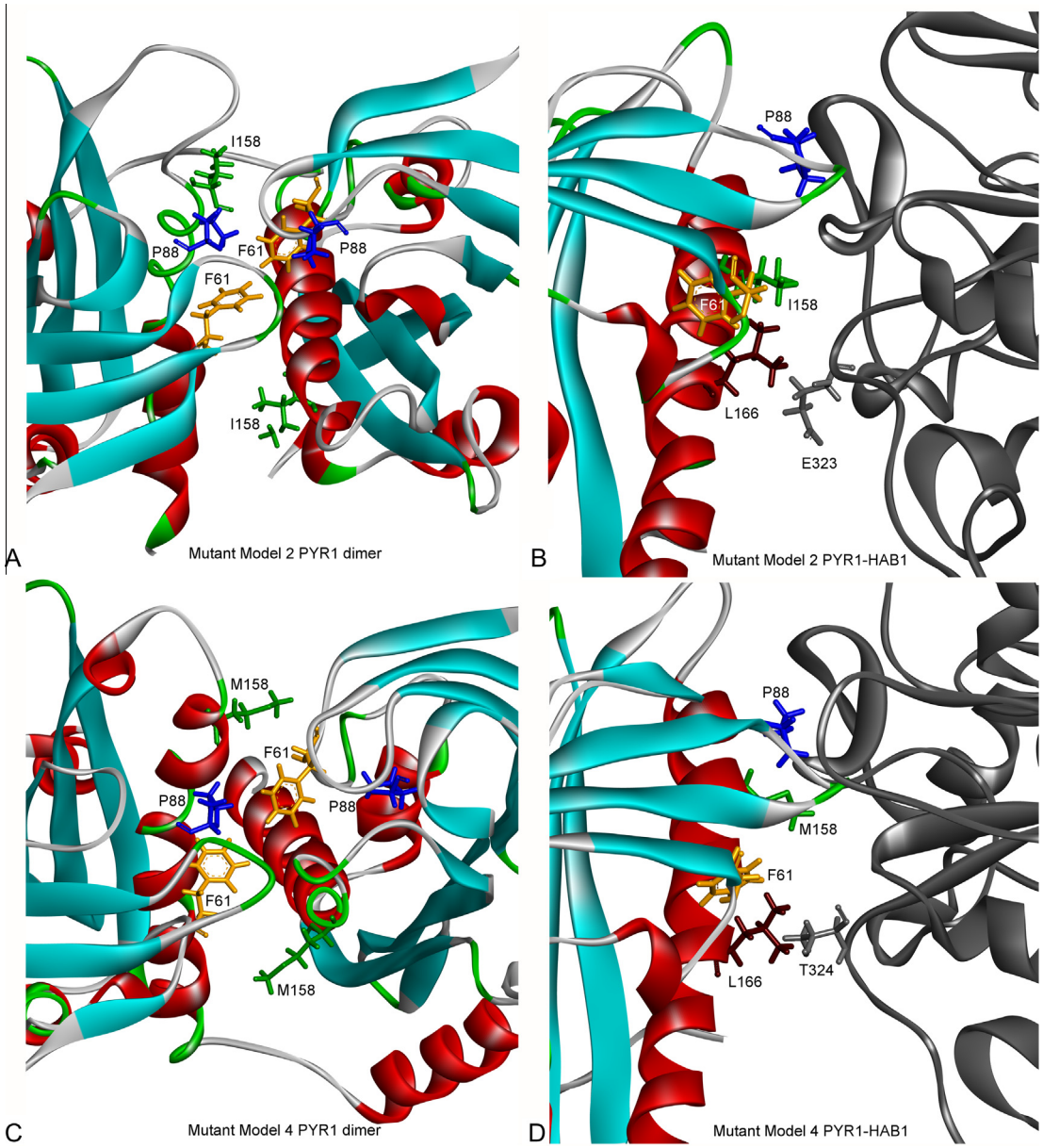

Fig. 7. Close up of the binding area for ABA-free dimer (A, C) and ABA-free PYR1–HAB1 complex (B, D) after 20 ns simulations for Model 2 (A, B) and Model 4 (C, D). The color scheme used is the same as for Fig. 3. In dimer, the orientation of side chain at F61 is similar as in Model 1, and in Model 2 it is slightly rotated. In PYR1–HAB1 complex, residue F61 leans towards PYR1 in both mutant models, and the bonding with E323, T324 and Y404 is not affected. In Model 4 strong bonding with T324 is observed. (For interpretation of the references to color in this figure legend, the reader is referred to the web version of this article.)

PYR1–HAB1 binding interfaces of in Models 2 and 4, respectively. As it can be seen in Fig. 7A and C, the binding interface for PYR1 mutant dimers of Models 2 and 4 is the same as in Model 1, with the exception of a slight rotation of F61 residues for Model 2 and changes in orientation of residue 158 for Model 4. In the PYR1–HAB1 binding interface (Fig. 7B and D for Models 2 and 4, respectively), the presence of other mutations than H60P does not change the orientation of residue F61, which remains rotated towards PYR1 receptor, allowing binding contacts with residues E323, T324, and Y404 of the phosphatase.

In Fig. 8 the flexibility of chains A in mutant dimers is compared with that of WT ABA-free WT dimer. According to the figure, there are quite significant differences among the profiles in Fig. 8. For both Models 2 and 4, the main chain flexibility in the areas of helix α5 and sheet β1 is lower, and that of loop Lβ7α5 is higher than in the WT construct. Also in Model 4 mutant dimer a lower flexibility of the latch in comparison with the WT construct has been found, which might be related to mutation V83F. Interestingly, in contrast to all mutant dimer Models 1–4, both 2ABA-bound and ABA-free WT dimers exhibit a minimum around PYR1 residue S152 and a maximum around PYR1 T156 in the flexibility profiles (see Figs. 4 and 8). In the mutant constructs, both the minimum of PYR1 flexibility at S152 and maximum at T156 are absent. As it can be seen elsewhere (Fig. 8 of Ref. [10]), these features are also absent for the WT PYR1–ABA–HAB1 complex. This suggests that the sets of mutations introduced may disrupt interactions of chain A loop Lβ7α5 with chain B in the dimers; however this loop is also less constrained in ABA-bound PYR1–HAB1 complex. Similarly to Model 1, the flexibility of chains B in mutant dimers of Model 2 and 4 (not shown) is very close to that of WT ABA-free dimer.

Fig. 9 presents difference maps for intra-molecular and inter-molecular correlations in Model 2 and Model 4 PYR1 dimers relative to the WT ABA-free dimer (control). When combined with other PYR1 mutations in Models 2 and 4, mutation H60P does

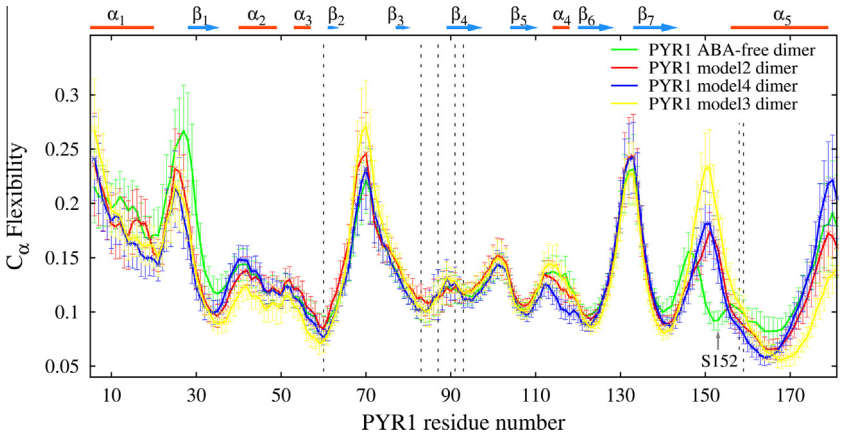

Fig. 8. PYR1 main chain flexibility profiles for chain A dimer constructs: WT ABA-free (green line), ABA-free Model 2 mutant (yellow line), ABA-free Model 3 mutant (blue line), and ABA-free Model 4 mutant (red line). Vertical dashed lines indicate the potential mutation sites and regions of phosphatase binding. (For interpretation of the references to color in this figure legend, the reader is referred to the web version of this article.)

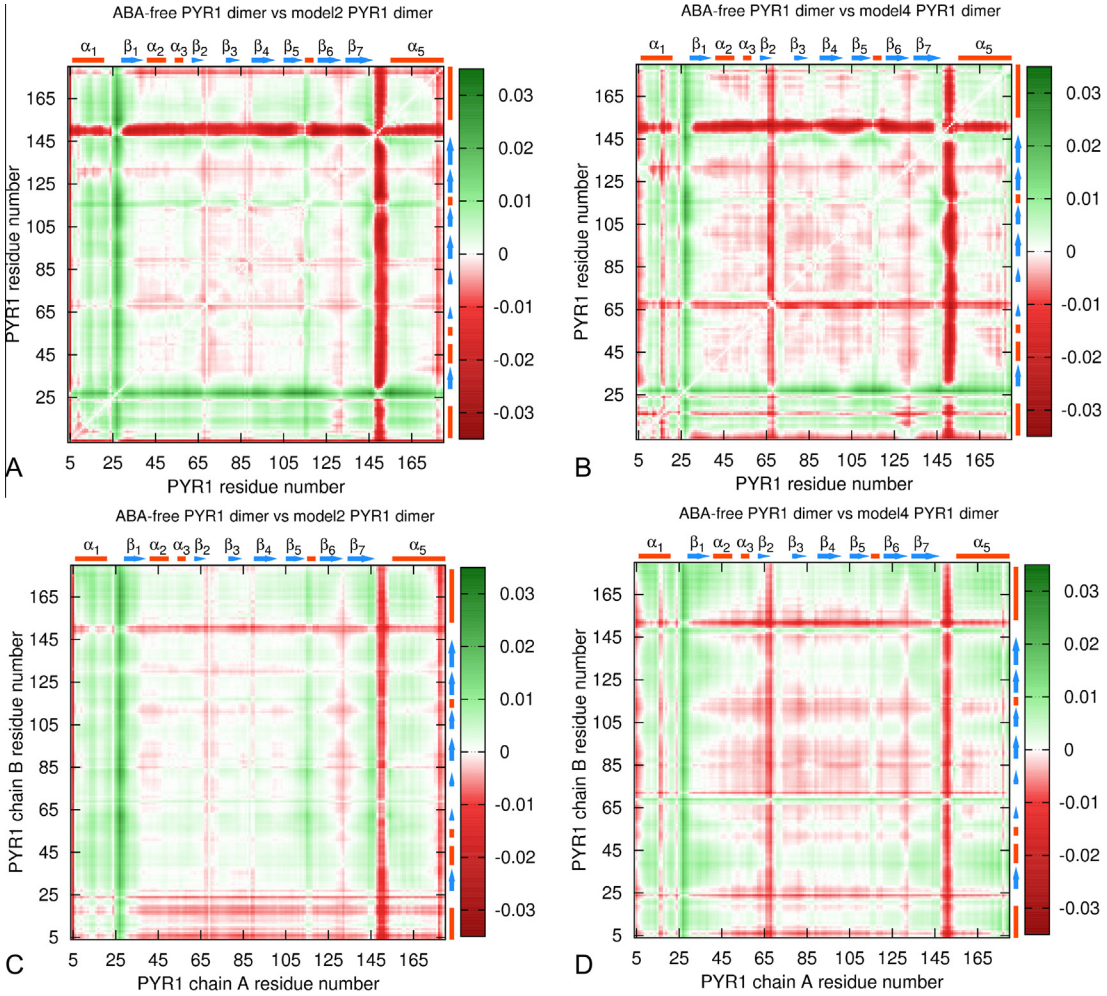

Fig. 9. Difference C_α atoms correlation maps for PYR1 dimer Model 2 (mutations H60P V83F M158I F159 V; panels A, C) and Model 4 (mutations D53E, H60P, V83I, L87I, F159 V; panels B, D) against the control WT PYR1 dimer construct: intra-receptor chain A C_α atoms difference correlation maps (A, B) and inter-molecular C_α atoms difference correlation maps (C, D). The color scheme is as in Fig. 6. (For interpretation of the references to color in this figure legend, the reader is referred to the web version of this article.)

not weaken intra-receptor correlations in the α5 region, which remains constrained by the other mutations (see Fig. 9A and B, respectively). However, intra-receptor correlations are weakened in the regions of Lβ6β7 loop, helix α1, and sheet β2 when mutation H60P is combined with D53E, V83I, L87I, and F159V (Model 4, see Fig. 9B), and around loops Lβ2β3, the gate, and Lβ6β7 when it is combined with mutations V83F, M158I, and F159V (Model 2, see Fig. 9A). The difference maps for inter-molecular correlations in dimer mutants (Fig. 9C and D) show an asymmetry in the dimer interactions. Distinctive for Model 2 mutant dimer, weak correla-

tions of helix α1 of chain B and chain A loop Lβ7α5 with most of residues in chains A and B, respectively have been observed (Fig. 9C). In turn for Model 4 mutant dimer, weakened correlations of chain A sheet β2 and chain B loop Lβ7α5 with most of the counterpart chains B and A, respectively, were found. However, inter-molecular correlations of chain A region 25–50 with most of chain B are more pronounced in Model 4 than in Model 2 (Fig. 9D). Combining mutation H60P with other mutations in Models 2 and 4 does not seem to significantly reduce correlations in helix α3 and most other regions in comparison with Model 1 (see Fig. S4B, Fig. 9C and D).

Comparison of PYR1 main chain flexibility profiles for Models 2 and 4 mutant PYR1–HAB1 complexes with WT PYR1–ABA–HAB1 complex (Fig. 10A) shows a very good agreement. In the case of Model 2, a slightly higher level of flexibility is observed for the gate and loop Lα3β2 region, while for Model 4, a slightly higher flexibility is found for the loop Lβ7α5. These differences are of similar magnitude as the difference in the receptor's main chain flexibility in PYR1–ABA–HAB1 and PYR1–HAB1 complexes as demonstrated elsewhere ([10], Fig. 8).

Fig. 11 (A–D) present PYR1–HAB1 intra-receptor (A, B) and inter-molecular (C, D) difference correlation maps for Model 2 (A, C) and Model 4 (B, D). For both Models 2 and 4, all correlations between helix α1 with most HAB1 regions, as well as inter-molecular correlations between HAB1's residue 223 with all PYR1 regions, are stronger than in the control construct WT PYR1–ABA–HAB1. In comparison with Model 2, Model 4 exhibits stronger intra-molecular (Fig. 11A and B) and inter-molecular (Fig. 11 C and D) correlations in the regions of PYR1 gate loop, whereas the correlations are weaker in the area of loop Lβ7α5, and also in the N-terminus region 1–6. Fig. 11C and D further demonstrate that Model 4 shows a higher level of inter-molecular correlations, in comparison with Model 2, between the areas of PYR1 gate, loop Lα3β2, and helix α5 with several broad HAB1 regions, especially with residues 306–320. The correlations with HAB residues 185–210, 235–260, 280–305, 340–350, 360–370, 380–415, 430–440, and 475–500 are also higher in Model 4 than in Model 2. In contrast, correlations of most PYR1 residues with HAB region 457–470 are stronger in Model 2 than in Model 4.

Overall, one can conclude that both Models 2 and 4 have the potential to improve the binding of PYR1 with PP2C in the absence of ABA ligand. Model 4 mutant exhibits more pronounced inter-molecular correlations with HAB's regions around residues 306–320, whereas Model 2 improves the correlations with the area around HAB residues 457–470. This is consistent with previous *in vitro* data [8] and the *in vitro* comparison presented herein demonstrating strong CA for Model 2 and weaker CA (evident only at higher ratios of receptor to phosphatase) for Model 4 (Fig. 2). The need for stronger constraints in the C-terminal helix α5 and loop Lβ7α5 may account for Model 4's lower relative CA, which could be achieved by replacing mutation H60P with L166F K170W positioned in the same region.

2.3.3. Model 3

Model 3 mutations comprise R50S, D53E, T93L, and V138R. Comparison of the main chain flexibility profile for ABA-free Model 3 dimer with that of the WT ABA-free dimer in Fig. 8 shows that the flexibility of the mutant dimer is somewhat different from that

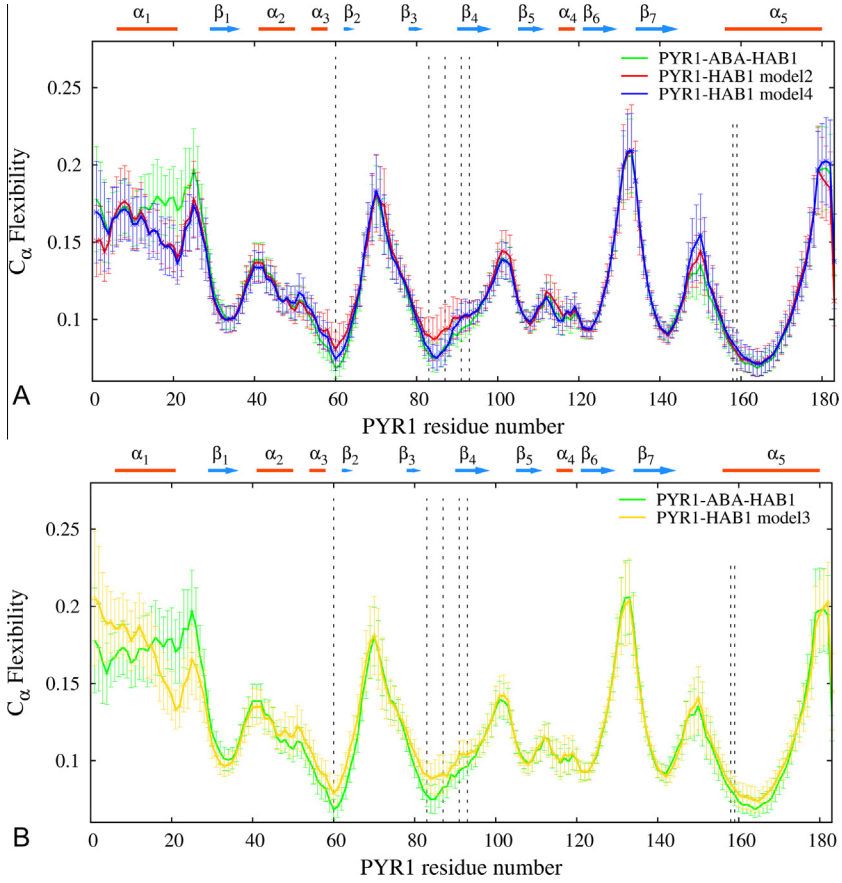

Fig. 10. PYR1 main chain flexibility profiles for PYR1–HAB1 constructs: (A) – ABA-bound WT (green line), ABA-free mutant H60P V83F M158I F159 V (Model 2) (red line) and ABA-free mutant D53E H60P V83I L87I F159 V (Model 4) (blue line); (B) – ABA-bound WT (green line), ABA-free mutant R50S D53E T93L V138R (Model 3) (yellow line). Vertical lines indicate the potential mutation sites and regions of phosphatase binding. (For interpretation of the references to color in this figure legend, the reader is referred to the web version of this article.)

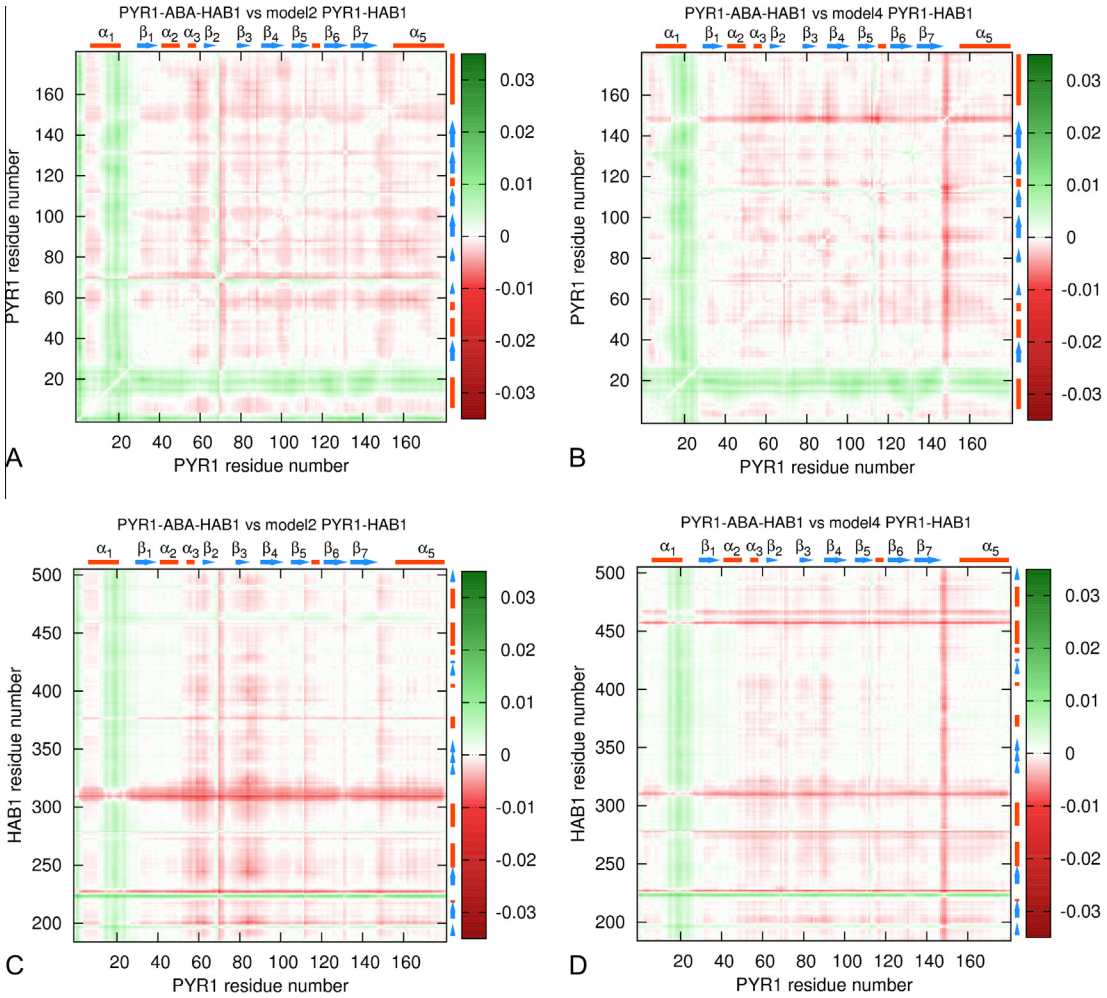

Fig. 11. Difference intra-molecular (A,B) and inter-molecular (C,D) C_α atoms correlation maps for Model 2 (mutations H60P V83F M158I F159 V; panels A and C) and Model 4 (mutations D53E, H60P, V83I, L87I, F159 V; panels B and D) PYR1–HAB1 complex against the control WT PYR1–ABA–HAB1 construct. The color scheme is as in Fig. 6. (For interpretation of the references to color in this figure legend, the reader is referred to the web version of this article.)

of ABA-free WT dimer, particularly in regions of loops Lα1β1, Lβ2β3, Lβ7α5, and helices α2 and α5. Interestingly, the flexibilities of chains A in both mutated Model 3 and WT ABA-free dimer exhibit a slightly higher flexibility of the latch in comparison to Model 2 and Model 4 mutants. At the same time, the flexibility of loops Lβ2β3 and Lβ7α5 are pronouncedly higher for Model 3 mutant than for WT dimer or other mutant models.

The difference intra-molecular and inter-molecular correlation maps for mutant Model 3 dimers against WT ABA-free dimer (control) are shown on Fig. 12A and B, respectively. Similarly to Models 2 and 4 (see Fig. 9A and B), intra-receptor correlations are improved for loop Lα1β1, and weakened for loop Lβ7α5 and sheet β2, in comparison to the control construct. Inter-molecular correlations for Model 3 against control show a strong increase in correlation for N-terminal part 7–60, helix α5 and a decrease in correlation around sheet β2 and loop Lβ7α5.

In Fig. 10B, main-chain flexibility of Model 3 receptor from PYR1–HAB1 complex is compared with that of the benchmark WT PYR1–ABA–HAB1 construct. Interestingly, although none of the mutation sites in Model 3 (R50S, D53E, T93L, and V138R) are close to the PYR1 ligand pocket or directly involved in the binding to HAB1, this mutation set reproduces very well the most important main chain flexibility features of the benchmark system WT PYR1–ABA–HAB1, except for a slightly higher flexibility in the gate area and helix α1. The difference in the flexibility profiles is comparable to that for WT PYR1–HAB1 and WT PYR1–ABA–HAB1 constructs described elsewhere [10]. The intra-receptor difference correlation map of Model 3 PYR1–HAB1 complex against WT PYR1–ABA–HAB control construct (Fig. 12C) is similar to that of Model 2 (Fig. 11A). Slightly stronger correlations in comparison to Model 2 are discernible in the regions of loops Lα1β1, Lβ1α2, and Lβ6β7, albeit pronouncedly weaker correlations are observed around helix α1. Difference inter-molecular correlation map for Model 3 PYR1–HAB1 complex against WT PYR1–ABA–HAB1 control (Fig. 12D) shows a weakening of correlations of PYR1 regions 1–15, 45–70, 75–95, and 150–175 with HAB1, and an increase in the correlations of loop Lα1β1 with most of HAB1 main chain. One can hypothesize that a certain change in the topology of the binding area is induced by mutating residues R50 and V138. These mutations may produce conformational changes which would constrain the loop Lβ7α5 of ABA-free PYR1, and also allow the receptor to adopt a conformation close to the ABA-bound one, thereby stabilizing the mutant PYR1–HAB1 complex (Fig. 12B). However no evidence of constitutive activity is observed for this model *in vitro* (Fig. 2), emphasizing overall that neither bulk destabilization of the dimer interface or stabilization of the HAB1 interface by altering main-chain flexibility features are in themselves sufficient to elicit CA. The importance of directly stabilizing the

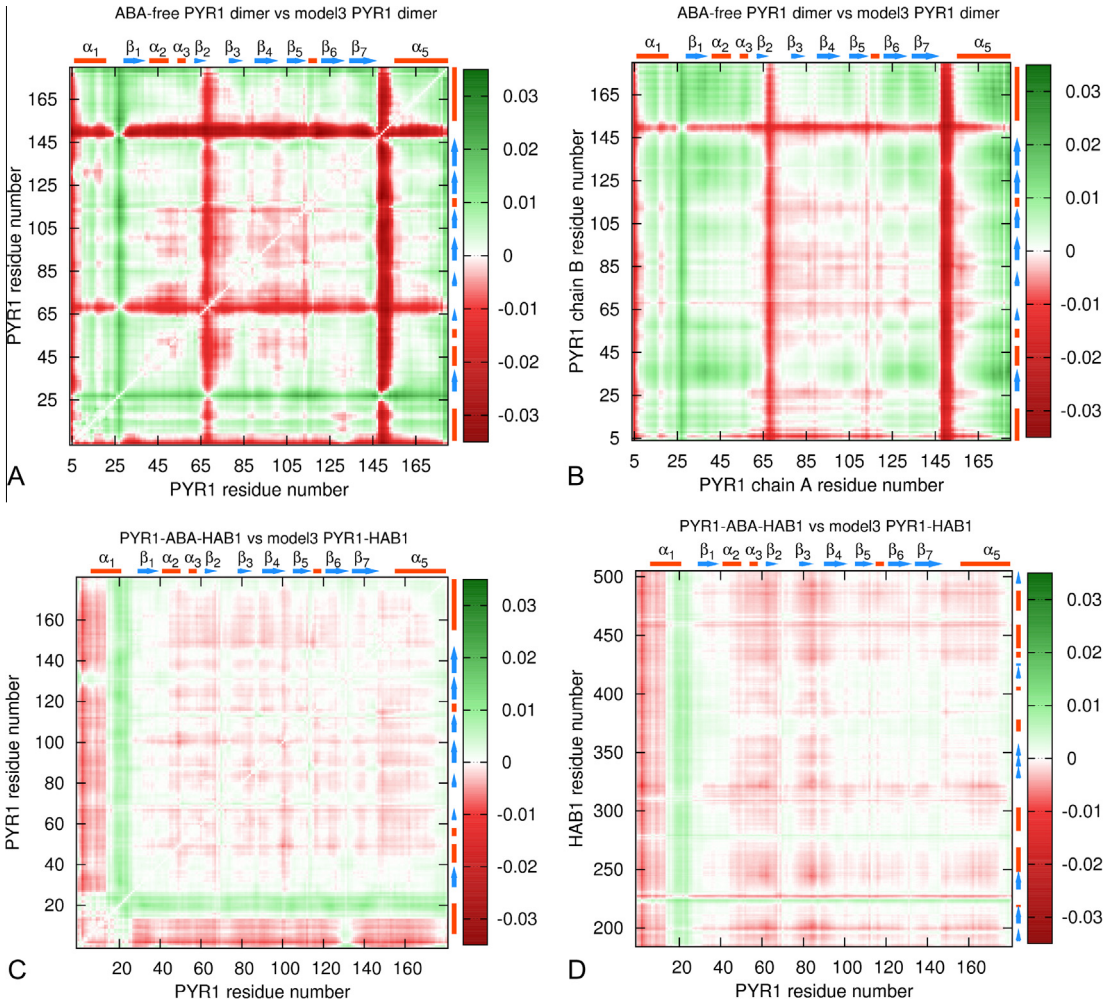

Fig. 12. Difference intra-molecular (A, C) and inter-molecular (B, D) chain A C_α atoms correlation maps for Model 3 (mutations R50S, D53E, T93L, V138R) dimer against the control WT dimer construct (A, B), and C_α atoms correlation maps for Model 3 PYR1–HAB1 complex against the control WT PYR1–ABA–HAB1 construct (C, D). The color schemes are as in Fig. 6. (For interpretation of the references to color in this figure legend, the reader is referred to the web version of this article.)

gate-region is emphasized. One can expect that Model 3 might be further improved by introducing the gate-stabilizing mutation V83I and dimer destabilizing mutation K170W.

In summary, an extensive series of MD simulations of the apo-form of mutagenized pyrabactin receptor PYR1 as a homodimer and in complex with HAB1 phosphatase are reported, and molecular motions (dynamics) aspects contributing to increased basal activity of pyrabactin receptors PYR1 against HAB1 investigated by the novel ECD method. Several sets of PYR1 mutations expected to favor the closed lid conformation in ABA-free PYR1, imitate strong inter- and intra-protein correlations of atomic motion observed in the benchmark WT PYR1–ABA–HAB1 complex, while destabilizing the ABA-free dimer, are assessed. The most significant differences in the flexibility profiles and correlation maps among the mutants as well as in comparison to their WT counterparts is found in the dimeric complexes. Although intra-receptor correlations are generally weaker in mutant PYR1–PYR1 dimers than in mutant PYR1–HAB1 complexes, the differences in correlations arising from the introduction of mutations are more pronounced for the dimer systems. Dynamics of HAB1-bound PYR1 were less responsive to the mutations. ABA-free mutant PYR1–HAB1 complexes and WT PYR1–ABA–HAB1 systems show almost identical main chain flexibility and mostly slight differences in intra-molecular and inter-molecular correlations. In general, the most significant changes of the dynamics in response to the mutations are observed around the loops Lα1β1, Lβ7α5, latch (Lβ5β6), and in sheet β2 of PYR1. Single dimer destabilizing mutation H60P (Model 1, [9]) was found to constrain the helix α1, sheet β2, and the loop Lα1β1 in the PYR1–HAB1 complex while destabilizing the loop Lβ7α5 and helix α5 in the dimer. When mutation H60P is combined with other three mutations V83F, M158I, F159V, the resulting Model 2 [8] acquires stronger intra-molecular and inter-molecular correlations in the areas of sheets β2 and β7, as well as at the loop Lα1β1 in both complexes, reproducing fairly well the intra-molecular correlation map of WT receptor in PYR1–ABA–HAB1 complex. While all mutation models considered reproduce very well the main chain flexibility profile of the benchmark WT PYR1–ABA–HAB1 construct, the most promising results were achieved both theoretically and experimentally with the sets of mutations H60P, V83F, M158I, F159V (Model 2, [8]) and D53E, H60P, V83I, L87I, F159V (Model 4). Simulations for Model 4 show that these mutations strengthen the binding between HAB1 and PYR1, especially in the regions of the gate and loop Lα3β2. The model also stabilizes helix α5 and improves the binding of it to the phosphatase. However, our simulations also suggest that this model may stabilize the interaction of PYR1 in the dimer, particularly involving residues 25–50. One can hypothesize that Model 4 could be further improved by replacing mutation H60P with L166F K170W. The latter is a promising double mutation not yet tested experimentally which may be expected to stabilize the

binding with phosphatase while decreasing the likelihood of PYR1 dimerization. The Model 3 mutation set R50S, D53E, T93L, and V138R is different from other models considered since none of the four mutations is in proximity to the ligand pocket or PP2C/dimer binding interface. Nevertheless, this set shows promising flexibility and binding performance, improving the correlation of loop Lα1β1 with HAB1, although not yielding any CA experimentally. One can hypothesize that the mutations distant from the binding surface, such as D53E or R50S, may affect stability of the receptor and orientation of residues on the binding interface. However in comparison to Model 2, Model 3 lacks correlations with HAB's region around residue 460, and it also appears to stabilize the region 25–50 of the dimer. We expect that Model 3 may be further improved by introducing gate-stabilizing mutation V83I and dimer destabilizing mutation K170W.

In contrast to earlier work reporting that triple and quadruple mutant combinations in the regions of the loop Lα3β2, the gate, and helix α5 (as implemented in Model 2) are sufficient for full receptor activation, the simulations reported herein suggest a more complex relationship. While simulations do suggest that the mutations induce promising changes of dynamics in the described regions, the simulations also suggest a possibility of an increased affinity of PYR1 for itself. Our data support the hypothesis that formation of dimers is in competition with the PP2C interactions for the mutated receptor constructs, and suggest that certain sets of mutations may favor one complex over the other. Our results also indicate that even a single mutation of PYR1 receptor may affect the dynamics of the entire PYR1–HAB1 complex, in particular the flexibility and inter-molecular correlations of distant from the binding surface regions of the phosphatase.

Overall, we anticipate that the described effects of mutations could be applicable for other dimeric pyrabactin-like-receptors, if considered in the context of individual sequence peculiarities. The mutations employed in Models 2 and 4 to enhance the binding to PP2C in particular might also improve activity in monomeric PYLs.

3. Materials and methods

3.1. In vitro mutant receptor activity assays

Details of protein preparation and assay are essentially as described previously [2]. The cDNA encoding *A. thaliana* PYR1 was cloned into the pET 100 vector (Invitrogen) to include an N-terminal His-Tag. This construct was introduced into *Escherichia coli* BL21 star (DE3), where recombinant expression of the PYR1 cDNA was induced by additional of 0.25 mM or 1.0 mM IPTG. HAB1 was cloned into pDEST17 (Invitrogen) also with an N-terminal HIS0tag, and introduced into *E. coli* BL21 AI cells, where its expression was induced by the addition of 0.2% arabinose. DNA encoding PYR1 with H60P, V83F, M158I, F159V (Set #3Model #2) mutations, PYR1 with R50S, D53E, T93L, V138R mutations (Set #4Model #3) and PYR1 with D53E, H60P, V83I, L87I, F159V mutations (Set #5Model #4) was synthesized and cloned into the pEX-N-His vector by Blue Heron Biotech, LLC (Bothell, WA, USA), which were introduced into *E. coli* BL21 star (DE3) where gene expression was induced by addition of 0.25 mM or 1.0 mM IPTG. All induced cultures were incubated overnight at 16 °C. The cell pellets were frozen in liquid nitrogen and stored at −80 °C. Frozen cell pellets were thawed and the final volume was made up to 20 mL using the lysis buffer (100 mM Tris pH 7.9, 100 mM NaCl, 0.3 mM $MnCl_2$ and 4 mM DTT) containing 10 mM imidazole. The cells were lysed using the French press at 1000 psi. The cell lysate was clarified by centrifuging at 17,000 rpm for 25 min at 4 °C. The supernatant was quickly removed and used for further purification. Purification was carried out by taking 4 mL of Ni–NTA (50% suspension) (QIAGEN) in a plastic column and washed thrice with 5 mL of lysis buffer containing 10 mM imidazole. The washed Ni–NTA resin was added to the cell lysate supernatant and incubated at 4 °C for 30 min. Elution of the bound protein was performed by adding 4 mL fractions of lysis buffer containing 150 mM imidazole till all proteins were eluted from the column. The ratio of HAB1:PYR1 was set at 1:2.5 and 1:25 with the HAB1 concentration set at 0.5 μM. PYR1 or mutant PYR1 was added to the phosphatase at 1.25 and 12.5 μM final concentrations respectively, in a 100 μl reaction mixture, in a buffer containing 100 mM Tris pH 7.9, 100 mM NaCl, 0.3 mM $MnCl_2$ and 4 mM DTT. This mixture was pre-incubated for 15 min at 30 °C and 1 mM substrate (1 mM 4-methylumbelliferyl phosphate) was added to the reaction mixture which was further incubated for 30 min at 30 °C. 1 μM (+) ABA was added to each receptor-phosphatase combination to test the functionality of each receptor. Phosphatase activity was determined by spectrofluorometric analysis with the excitation wavelength was 355 nm and the emission wavelength at 460 nm.

3.2. The structure models and molecular dynamics simulations

3D structures of the complexes PYR1–ABA–HAB1 and pyrabactin (PYV) bound PYR1 dimer were taken from the Protein Data Bank, PDB ID 3QN1, and 3NJO chains A and B, [20,15–16] and prepared for simulations, see comments in Table 2 and Ref. [10]. In the crystallographic dimer structure (PDB ID 3NJO) reverse S88P mutation and ligands PYV/P2M removal/replacement with two ABA have been done. Mutant PYR1 constructs were produced *in silico* by mutating the ligand-removed wild type structures (with proline residue at position 88) with Accelrys Discovery Studio software [21]. All constructed regions were optimized. Some of the mutated constructs were additionally *in vacuo* minimized without restraints in order to eliminate steric clashes. Minimizations, equilibrations and production MD simulations were carried out using Gromacs v4.0.7 package [22] with OPLS force fields. Starting models of WT PYR1 complexes and mutant systems were minimized *in vacuo* for 10000 steps of steepest descent minimization, after which the systems were solvated and counterions added. Next, steepest descent minimization was carried out as described elsewhere [10], followed by system heating employing the Berendsen thermostat. NVT equilibration was made subsequently. The last equilibration step and the production simulations were conducted at 310 K temperature and 1 atm pressure with isotropic pressure coupling (NPT ensemble) and bond length restrained with the LINCS algorithm

Table 2
List of 3D PYR1 constructs taken from PDB and modeled *in silico*, which were used for MD simulations and analysis.

Construct	PYR1 dimer	PYR1–HAB1 complex
Ligand free	PYV/P2M extracted from 3NJO [16], S88 replaced with P88	ABA extracted from 3QN1.pdb with parts of HAB1 reconstructed [15]
Ligand-bound	(1) PYV/P2M replaced with two ABA and S88 replaced with P88 in 3NJO [16] (2) PYV replaced with one ABA, P2M removed, and S88P mutation in 3NJO	3QN1.pdb [15], with parts of HAB1 reconstructed
Apo-mutants	Mutant models based on chains A and B of 3NJO with PYV/P2M extracted, and S88P mutation [16]	Mutant models based on 3QN1.pdb, ABA extracted with parts of HAB1 reconstructed [15]

with a fourth order of expansion. Further details of our MD protocols can be found in Ref. [10]. Overall, the mutant PYR1 dimer systems consisted of approximately 6000 atoms (or 350 residues), whereas the mutant PYR1–HAB1 systems comprised approximately 8000 atoms (500 residues). The explicit water solvent contained 100000–125000 atoms. The production simulations were performed with 1 fs time steps from 20 ns to 50 ns depending on the system, and snapshots saved every 20 fs in order to analyze the essential collective dynamics.

3.3. Essential collective dynamics (ECD) of PYR1 complexes

The mutagenized PYR1 constructs were analyzed as homodimers or in the PYR1–PP2C complex employing ECD methodology, as described earlier [10]. ECD is a novel method that allows probing of persistent structural properties of proteins based on short (a few hundreds of picoseconds) all-atom molecular dynamic trajectories [11–14]. The ECD method relies upon a recently developed statistical-mechanical framework [11,13], according to which a macromolecule can be described by a set of generalized Langevin equations with essential collective coordinates, which can be deduced by applying principal component analysis (PCA) on MD trajectories. In this framework, the protein can be represented by an all-atom image $\{\vec{r}_1, \vec{r}_2, \ldots, \vec{r}_N\}$ in the $3K$ dimensional space of essential collective coordinates, where N is the number of atoms in the protein, and K is the number of essential components (PCA eigenvectors) which sample approximately 90% or more of the total displacement in a MD trajectory of the protein. In the protein's image, the distances between atoms $d_{ij} = |\vec{r}_i - \vec{r}_j|$ represent the degree of dynamic correlation: short distances d_{ij} indicate that atoms i and j move coherently regardless of their proximity in 3D structure, whereas larger distances represent a relatively independent motion. A suite of simple structural descriptors, such as main chain flexibility profiles, domains of correlated motion, and intermolecular and intra-molecular correlation maps have been derived within the ECD framework, validated against X-ray [10] and NMR [11–14,23] structural data, and successfully employed to analyze dynamics of proteins and protein–ligand complexes [10,12,14,23–25]. The ECD method does not require exhaustive sampling of the conformational space in order to draw accurate predictions. Short sub-nanosecond segments of MD trajectories are usually sufficient for a compatibility of the predictions with NMR experiments representing significantly longer time regimes [11–14,23].

The dynamics of PYR1 constructs were characterized primarily employing ECD derived correlation maps and flexibility profiles. The ECD correlation maps represent distances d_{ij} between images of atoms in the space of essential collective coordinates, and the main chain flexibility profiles $F_i^{C_\alpha} = |\vec{r}_i^{C_\alpha} - \vec{\varepsilon}_i^{C_\alpha}|$ are defined as distances between images of C_α atoms, $\vec{r}_i^{C_\alpha}$, and the centroid over the images of all C_α atoms, $\vec{\varepsilon}_i^{C_\alpha} = \frac{1}{N_{C_\alpha}} \sum \vec{r}_i^{C_\alpha}$. A more detailed discussion of the ECD descriptors can be found elsewhere [12,14].

Here, ECD main chain flexibility profiles and correlation maps were obtained with $K = 20$. For each construct considered, we employed 100 segments, each of 20 fs, from the last 20 ns of the MD trajectories, to obtain the averaged data for the analysis. The ECD method allows analyzing the dynamics of both main-chain [10–12,14,23,25] and side-chains [14,24,25] of a protein; however in this work we have concentrated on main-chain C_α atoms since their motion represents the most robust trends of the collective dynamics.

In our comparative analysis of PYR1 mutants, we have extensively employed the difference correlation maps relative to a control system. We define the difference correlation descriptor by

$$\Delta d_{ij}^{AC} = -(d_{ij}^{A} - d_{ij}^{C}), \quad (1)$$

where d_{ij}^{A} and d_{ij}^{C} represent the degree of dynamic correlation between C_α atoms i and j in the analyzed construct and in the control construct, respectively. With this definition, positive values of difference descriptor Δd_{ij}^{AC} indicate that correlation is stronger in the analyzed system than in the control, and negative values suggest that correlation of is weaker than in the control. By doing such analysis, subtle differences of the molecular dynamics can be revealed, which are difficult to capture by other methods.

Author contributions

The manuscript was written through contributions of all authors. All authors have given approval to the final version of the manuscript.

Conflict of interest

The authors declare no financial conflict of interests.

Acknowledgements

The authors thank Oliver Stueker, Bilkiss Issack, Taras Fito, Mark Berjanskii, and Nikolay Blinov for their programming contributions and stimulating discussions. Molecular images were created using the VMD package [26] and Accelrys VS package [21]. The work was supported by the National Research Council (NRC) of Canada, Genomics and Health Initiative Program.

Appendix A. Supplementary data

Supplementary data associated with this article can be found, in the online version, at http://dx.doi.org/10.1016/j.fob.2014.05.001.

References

[1] Park, S.Y., Fung, P., Nishimura, N., Jensen, D.R., Fuji, H., Zhao, Y., Lumba, S., Santiago, J., Rodriguez, A., Chow, T.F., Alfred, S.E., Bonetta, D., Finkelstein, R., Provart, N.J., Desveaux, D., Rodriguez, P.L., McCourt, P., Zhu, J.K., Schroeder, J.I., Volkman, B.F. and Cutler, S.R. (2009) Abscisic acid inhibits type 2C protein phosphatases via the PYR/PYL family of START proteins. Science 324, 1068–1071.

[2] Ma, Y., Szostkiewicz, I., Korte, A., Moes, D., Yang, Y., Christmann, A. and Grill, E. (2009) Regulators of PP2C phosphatase activity function as abscisic acid sensors. Science 324, 1064–1068.

[3] Santiago, J., Dupeux, F., Round, A., Antoni, R., Park, S.Y., Jamin, M., Cutler, S.R., Rodriguez, P.L. and Marquez, J.A. (2009) The abscisic acid receptor PYR1 in complex with abscisic acid. Nature 462, 665–668.

[4] Miyazono, K., Miyukawa, T., Sawano, Y., Kubota, K., Kang, H.J., Asano, A., Miyauchi, Y., Takahashi, M., Zhi, Y., Fujita, Y., Yoshida, T., Kodaira, K.S., Yamaquchi-Shinozaki, K. and Tanokura, M. (2009) Structural basis of abscisic acid signaling. Nature 462, 609–614.

[5] Melcher, K., Ng, L.M., Zhou, X.E., Soon, F.F., Xu, Y., Suino-Powell, K.M., Park, S.Y., Weiner, J.J., Fujii, H., Chinnusamy, V., Kovach, A., Li, J., Wang, Y., Li, J., Peterson, F.C., Jensen, D.R., Young, E.L., Volkman, B.F., Cutler, S.R., Zhu, J.K. and Xu, H.E. (2009) A gate-latch-lock mechanism for hormone signaling by abscisic acid receptors. Nature 462, 602–608.

[6] Melcher, K., Xu, Y., Ng, L.M., Zhou, X.E., Soon, F.F., Chinnusamy, V., Suino-Powell, K.M., Kovach, A., Tham, F.S., Cutler, S.R., Li, J., Yong, E.L., Zhu, J.K. and Xu, H.E. (2010) Identification and mechanism of ABA receptor. Nat. Struct. Mol. Biol. 17, 1102–1108.

[7] Hao, Q., Yin, P., Li, W., Wang, L., Yan, C., Lin, Z., Wu, J.Z., Wang, J., Yan, S.F. and Yan, N. (2011) The molecular basis of ABA-independent inhibition of PP2C by a subclass of PYL proteins. Mol. Cell 42, 662–672.

[8] Mosquna, A., Peterson, F.C., Park, S.Y., Lozano-Juste, J., Volkman, B.F. and Cutler, S.R. (2011) Potent and selective activation of abscisic acid receptors in vivo by mutational stabilization of their agonist-bound conformation. Proc. Natl. Acad. Sci. U.S.A. 108, 20838–20843.

[9] Dupeux, F., Santiago, J., Betz, K., Twycross, J., Park, S.Y., Rodriguez, L., Gonzalez-Guzman, M., Jensen, M.R., Krasnogor, N., Blackledge, M., Holdsworth, M., Cutler, S.R., Rodriguez, P.L. and Marquez, J.A. (2011) A thermodynamic switch modulates abscisic acid receptor sensitivity. EMBO J. 30, 4171–4184.

[10] Dorosh, L., Kharenko, O.A., Rajagopalan, N., Loewen, M.C. and Stepanova, M. (2013) Molecular mechanisms in the activation of abscisic acid receptor PYR1. PLoS Comput. Biol. 9 (6), e1003114.

[11] Stepanova, M. (2007) Dynamics of essential collective motions in proteins: theory. Phys. Rev. E 76. 05191.
[12] Blinov, N., Berjanskii, M., Wishart, D.S. and Stepanova, M. (2009) Structural domains and main-chain flexibility in prion proteins. Biochemistry 48, 1488–1497.
[13] Potapov, A. and Stepanova, M. (2012) Conformational modes in biomolecules: dynamics and approximate invariance. Phys. Rev. E 85. 020901(R).
[14] Issack, B.B., Berjanskii, M., Wishart, D.S. and Stepanova, M. (2012) Exploring the essential collective dynamics of interacting proteins: application to prion protein dimers. in: Proteins Struct. Funct. Bioinf. 80, 1847–1865.
[15] Dupeux, F., Antoni, R., Betz, K., Santiago, J., Gonzalez-Guzman, M., Rodriguez, L., Rubio, S., Park, S.Y., Cutler, S.R., Rodriguez, P.L. and Marquez, J.A. (2011) Modulation of abscisic acid signaling in vivo by an engineered receptor-insensitive protein phosphatase type 2C allele. Plant Physiol. 156, 106–116.
[16] Peterson, F.C., Burgie, E.S., Park, S.Y., Jensen, D.R., Weiner, J.J., Bingman, C.A., Chang, C.E., Cutler, S.R., Phillips Jr, G.N. and Volkman, B.F. (2010) Structural basis for selective activation of ABA receptors. Nat. Struct. Mol. Biol. 17, 1109–1113.
[17] Nishimura, N., Hitomi, K., Arvai, A.S., Rambo, R.P., Hitomi, C., Cutler, S.R., Schroeder, J.I. and Getzoff, E.D. (2009) Structural mechanism of abscisic acid binding and signaling by dimeric PYR1. Science 326, 1373–1379.
[18] Yin, P., Fan, H., Hao, Q., Yuan, X., Wu, D., Pang, Y., Yan, C., Li, W., Wang, J. and Yan, N. (2009) Structural insights into the mechanism of abscisic acid signaling by PYL proteins. Nat. Struct. Mol. Biol. 16, 1230–1236.
[19] Creighton, T. (1984) Proteins, Freeman, San-Francisco.
[20] Bernstein, F.C., Koetzle, T.F., Williams, G.J., Meyer, E.F., Brice Jr, M.D., Rodgers, J.R., Kennard, O., Shimanouchi, T. and Tasumi, M. (1977) The Protein Data Bank: a computer-based archival file for macromolecular structures. J. Mol. Biol. 112, 535–542.
[21] Accelrys Software Inc. [Online]. <http://accelrys.com/> (accessed May 26, 2011).
[22] Berendsen, H.J.C., van der Spoel, D. and van Drunen, R. (1995) GROMACS – a message-passing parallel molecular dynamics implementation. Comput. Phys. Commun. 91, 43–56.
[23] Santo, K.P., Berjanskii, M., Wishart, D.S. and Stepanova, M. (2011) Comparative analysis of essential collective dynamics and NMR-derived flexibility profiles in evolutionary diverse prion proteins. Prion 5, 188–200.
[24] Barakat, K., Issack, B.B., Stepanova, M. and Tuszynski, J. (2011) Effects of temperature on the p53-DNA binding interactions and their dynamical behavior: comparing the wild type to the R248Q mutant. PLoS One 6, e27651.
[25] Stueker, O., Ortega, V.A., Goss, G.G. and Stepanova, M. (2014) Understanding interactions of functionalized nanoparticles with proteins: a case study on lactate dehydrogenase. Small 10, 2006–2021.
[26] Humphrey, W., Dalke, A. and Schulten, K. (1996) VMD: visual molecular dynamics. J. Mol. Graph. 14 (33–8), 27–28.